Astrocytic glycogen accumulation drives the pathophysiology of neurodegeneration in Lafora disease

Jordi Duran,[1,2] Arnau Hervera,[3,4,5,6] Kia H. Markussen,[7] Olga Varea,[1] Iliana López-Soldado,[1] Ramon C. Sun,[8] Jose Antonio del Río,[3,4,5,6] Matthew S. Gentry[7] and Joan J. Guinovart[1,2,9]

ABSTRACT

The hallmark of Lafora disease, a fatal neurodegenerative disorder, is the accumulation of intracellular glycogen aggregates, called Lafora bodies. Until recently, it was widely believed that brain Lafora bodies were present exclusively in neurons and thus that Lafora disease pathology derived from their accumulation in this cell population. However, recent evidence indicates that Lafora bodies are also present in astrocytes. To define the role of astrocytic Lafora bodies in Lafora disease pathology, we deleted glycogen synthase specifically from astrocytes in a mouse model of the disease (malin^{KO}). Strikingly, blocking glycogen synthesis in astrocytes—thus impeding Lafora bodies accumulation in this cell type—prevented the increase in neurodegeneration markers, autophagy impairment, and metabolic changes characteristic of the malin^{KO} model. Conversely, mice that overaccumulate glycogen in astrocytes showed an increase in these markers. These results unveil the deleterious consequences of the deregulation of glycogen metabolism in astrocytes and change the perspective that Lafora disease is caused solely by alterations in neurons.

Author affiliations:

1 Institute for Research in Biomedicine (IRB Barcelona), The Barcelona Institute of Science and Technology, Barcelona, 08028, Spain

2 Centro de Investigación Biomédica en Red de Diabetes y Enfermedades Metabólicas Asociadas (CIBERDEM), Madrid, 28029, Spain

3 Institute for Bioengineering of Catalonia (IBEC), The Barcelona Institute of Science and Technology, Barcelona, 08028, Spain

4 Centro de Investigación Biomédica en Red sobre Enfermedades Neurodegenerativas (CIBERNED), Madrid, 28031, Spain

5 Department of Cell Biology, Physiology and Immunology, Universitat de Barcelona, Barcelona, 08028, Spain

6 Institute of Neurosciences, University of Barcelona, 08028 Barcelona, Spain

7 Department of Molecular and Cellular Biochemistry, University of Kentucky College of Medicine, Lexington, KY, 40536, USA

8 Department of Neuroscience, University of Kentucky College of Medicine, Lexington, KY, 40536, USA

9 Department of Biochemistry and Molecular Biomedicine, Universitat de Barcelona, Barcelona, 08028, Spain

Correspondence to: Dr Jordi Duran

IRB Barcelona, Baldiri i Reixac, 10, Barcelona 08028, Spain

E-mail: jordi.duran@irbbarcelona.org

Running title: Role of astrocytes in Lafora disease

Keywords: Lafora disease; glycogen; neurodegeneration; neuroinflammation; epilepsy

ABBREVIATIONS

CAL – corpora amylacea-like bodies

LBs – Lafora bodies

LD – Lafora disease

MGS – muscle glycogen synthase

nLBs – neuronal Lafora bodies

INTRODUCTION

Glycogen, a branched polymer of glucose, is the only energy reservoir of the brain and it plays important roles in this organ[1,2]. Recent work has demonstrated that astrocytes and neurons have an active glycogen metabolism that is key to their normal functioning[1-5]. However, in some conditions, glycogen accumulates abnormally in the brain[6,7]. The most striking example of this is Lafora disease (LD), a neurodegenerative condition that presents as a severe progressive myoclonus epilepsy characterized by the presence of glycogen aggregates, called Lafora bodies (LBs). LBs are intracellular, aberrant glycogen aggregates that accumulate in several tissues, including the brain. LD patients initially present with myoclonic jerks followed by epileptic seizures resistant to treatment. This phase is followed by rapid neurodegeneration, dementia and finally death within 5-10 years after the onset[8,9].

LD is caused by mutations in one of two genes: *EPM2A* encoding laforin, a dual-specificity phosphatase, and *EPM2B* encoding malin, an E3 ubiquitin ligase. Mutations in either gene cause the same disease, thus indicating that the two proteins form a functional complex[10-12]. Blocking brain glycogen synthesis in mouse models of LD prevents the progression of the disease[13-15]. This observation thus demonstrates that the accumulation of glycogen aggregates underlies the etiopathology of all aspects of the disease.

Until recently, it was widely assumed that glycogen aggregates in the brains of LD patients and animal models accumulate exclusively in neurons[8,16] and thus neuronal LBs were considered to be solely responsible for LD pathophysiology. In this regard, we demonstrated that glycogen accumulation in neurons induces their death by apoptosis[17]. However, there is a growing body of evidence showing that LBs are also present in astrocytes. In 2011, we reported the presence of glycogen aggregates in both neurons and astrocytes of the malin knockout mouse model ($malin^{KO}$)[18]. More recently, we[19] and others[20] further described the presence of these aggregates in astrocytes of LD mouse models, by means of co-localization with cell-type-specific

markers. We classified the glycogen aggregates in the brain into two types: astrocytic corpora amylacea-like bodies (CAL) and neuronal Lafora bodies (nLBs). The former are analogous to corpora amylacea, which are glycogen aggregates that normally accumulate in aged brains[21]. In this regard, CAL: i) are polymorphic; ii) are found grouped in clusters; and iii) co-localize with astrocytic markers. In contrast, nLBs: i) are round and normally larger than CAL; ii) co-localize with neuronal markers; and iii) are not present in clusters but are isolated in the form of a single aggregate close to the neuronal nucleus[19].

To determine which cell type contributes to the different LD pathophysiologies, we generated a malin^{KO} mouse model in which the enzyme responsible for glycogen synthesis in the brain, namely the muscle isoform of glycogen synthase (MGS), is specifically ablated from astrocytes (malin^{KO}+MGS$^{Gfap\text{-}KO}$). Our results show that most glycogen aggregates observed in the brains of malin^{KO} mice are not present in the malin^{KO}+MGS$^{Gfap\text{-}KO}$ animals, thereby proving that these aggregates accumulate in astrocytes. Furthermore, the latter animals did not show an increase in neurodegeneration markers, autophagy impairment, or the metabolic changes typical of the malin^{KO} mouse model, indicating that these symptoms are a consequence of the accumulation of astrocytic CAL. To corroborate these results, we generated mice that overaccumulate glycogen specifically in astrocytes. These animals also showed an increase in neurodegeneration markers. In contrast, the epileptic phenotype was not corrected in malin^{KO}+MGS$^{Gfap\text{-}KO}$ mice, indicating that the accumulation of astrocytic LBs is not the main driver of this symptom. All together, these results demonstrate the contribution of astrocytes to the pathology of LD and have important implications regarding the role of astrocytic metabolism in neurodegenerative diseases.

MATERIALS AND METHODS

Generation of malin^{KO}+MGS$^{Gfap\text{-}KO}$ and 9A-MGS^{Gfap} mice

To generate a malin^{KO} mouse that is unable to accumulate glycogen in astrocytes (malin^{KO}+MGS$^{Gfap\text{-}KO}$), we took advantage of our MGS conditional knockout (KO) model, which is based on Cre-Lox technology[1]. The ablation of MGS specifically in

astrocytes ($MGS^{Gfap\text{-}KO}$) was achieved by crossing this conditional KO with mice expressing Cre Recombinase under the control of a Gfap promoter (Gfap-Cre mice)[5]. The resulting mouse was then crossed with $malin^{KO}$, the descendants were genotyped for the three alleles involved (malin, MGS and Cre), and the suitable genotypes were intercrossed to generate all the experimental groups. To generate mice that overaccumulate glycogen in astrocytes (9A-MGS^{Gfap} mice), we took advantage of our mouse model conditionally expressing a non-inactivatable form of MGS (9A-MGS)[17]. Again, we combined this animal with Gfap-Cre mice to drive the expression of 9A-MGS specifically to astrocytes.

Animal studies

All procedures were approved by the Barcelona Science Park's Animal Experimentation Committee and were carried out following Spanish (BOE 34/11370-421, 2013) and European Union (2010/63/EU) regulations, and The National Institutes of Health guidelines for the care and use of laboratory animals. Mice were maintained in collective cages (up to five animals per cage) on a 12/12 h light/dark cycle under specific pathogen-free conditions in the Animal Research Center at the Barcelona Science Park. Animals were allowed access ad libitum to commercial mouse chow and water. After weaning at 3 weeks of age, tail clippings were taken for genotyping by qPCR (performed by Transnetyx).

Biochemical analyses

Mice were deeply anesthetized and then decapitated, and the brain was quickly removed and placed in liquid nitrogen. Whole brains were then pulverized in liquid nitrogen. For western blot analyses, fractions of the powder were weighed and homogenated in 10 volumes of ice-cold buffer containing 25 mM Tris–HCl (pH 7.4), 25 mM NaCl, 1% Triton X-100, 0.1% SDS, 0.5 mM EGTA, 10 mM sodium pyrophosphate, 1 mM sodium orthovanadate, 10 mM NaF, 25 nM okadaic acid and a protease inhibitor cocktail tablet (Roche). Homogenates were loaded in 10% acrylamide gels for SDS-PAGE and transferred to Immobilon membranes (Millipore). Antibodies against MGS (from Cell Signaling), laforin (a gift from Dr Santiago Rodríguez de Córdoba) and p62 (from Progen) were used. Proteins were detected by

the ECL method (Immobilon Western Chemiluminescent HRP Substrate, Millipore). Loading control of the western blot membrane was performed using the Revert total protein stain. For glycogen measurements, fractions of the brain powder were boiled in 30% KOH for 15 min and glycogen was determined by an amyloglucosidase-based assay as previously described[3]. For quantitative (q)PCR, total RNA was isolated from fractions of brain powder using Trizol reagent (Life Technologies, Carlsbad, CA, United States), purified with an RNeasy Mini Kit (Qiagen, Hilden, Germany) and treated with DNase I (Qiagen) to degrade genomic DNA. Reverse transcription was performed using qScript cDNA Synthesis Kit (Quanta Biosciences, Beverly, MA, United States). qPCR was performed using a Quantstudio 6 Flex (Applied Biosystems, Foster City, CA, United States). The following mouse-specific SYBRgreen sets of primers (Sigma, Madrid, Spain) were used: C3 (forward: 5'-TCCTGAACTGGTCAACATGG-3'; reverse: 5'-AAACTGGGCAGCACGTATTC-3'); Ccl2 (forward: 5'-AGGTGTCCCAAAGAAGCTGTAG-3'; reverse: 5'-TCTGGACCCATTCCTTCTTG-3'); Lcn2 (forward: 5'-CAGAAGGCAGCTTTACGATG-3'; reverse: 5'-CCTGGAGCTTGGAACAAATG-3'); Cxcl10 (forward: 5'-CCGTCATTTTCTGCCTCATC-3'; reverse: 5'-CTCGCAGGGATGATTTCAAG-3') and β-actin (Actβ), used as a housekeeping gene (forward: 5'- ACTGAGCTGCGTTTTACACC-3'; reverse: 5'-AGCCATGCCAATGTTGTCTC-3'). Samples were run as triplicates. For representation of the results, dCt was calculated as Ct (Actβ)-Ct (gene of interest), and average dCt from control hippocampus was used to calculate ddCT. Results are expressed as 2ˆddCt in relative units.

Histology

Animals were anesthetized and perfused transcardiacally with phosphate buffered saline (PBS) containing 4% of paraformaldehyde (PF). Brains were removed, postfixed overnight with PBS 4% PF and embedded in paraffin. Paraffin coronal brain sections (3 μm thick) were cut using a Leica microtome. PAS staining was carried out using an Artisanlink Pro machine (AR16592-2 kit, Artisan, Dako, Agilent). Immunostainings were performed using primary antibodies against MGS (ref. 3886 from Cell Signaling), Gfap (ref. MAB360, from Merck Millipore), and Iba1 (ref. 019-19741 from WAKO). The secondary antibodies used were Goat Anti-Mouse (P0447,

Dako, Agilent) or a BrightVision Poly-HRP-Anti Rabbit IgG (Immunologic, DPVR-110HRP). Antibody complexes were revealed with 3-3-diaminobenzidine (K3468, Dako) with the same time exposure per antibody. Brightfield images were acquired with a NanoZoomer-2.0 HT C9600 digital scanner (Hamamatsu) equipped with a 20X objective. All images were visualized with the NDP.view 2 software (Hamamatsu, Photonics, France). QuPAth software was used to perform image analysis for quantifying the area of Gfap- or Iba1-positive pixels[22] in hematoxylin-counterstained sections. The region of interest (hippocampus area) was selected manually. Results are the percentage of the positive area following the equation: *% of positive pixels = positive pixels *100 / (positive + negative pixels)*.

Assessment of kainate-induced epilepsy

Animals were placed in individual cages and administered three consecutive i.p. injections of kainate (8 mg/kg per dose, 24 mg/kg total), one every 30 min from the onset of the experiment in order to induce convulsive non-lethal seizures. Seizure stages after kainate injections were evaluated as described previously[23-25]. After the first kainate injections, the animals developed hypoactivity and immobility (Stage I–II). After successive injections, hyperactivity (Stage III) and scratching (Stage IV) were often observed. Some animals progressed to a loss of balance control (Stage V) and further chronic whole-body convulsions (Stage VI). Extreme behavioural manifestations such as uncontrolled hopping or "popcorn behaviour" and continuous seizures (more than 1 minute without control of body movement) were included in Stage VI. All behavioural assessments were performed blind to the experimental group (genotype) in situ, and were also recorded and re-analyzed blind to the first analysis. Analysis consisted of recording the time spent until the onset of the first seizure, the number of seizures per animal and the time spent in each stage by each animal.

GCMS quantitation of metabolites

Brain metabolomics analysis was performed based on our previously established methods[26-28]. Twenty milligrams of each pulverized tissue were extracted in 1ml of 50% methanol containing 20 μM L-norvaline as an internal procedural control and

separated into polar (aqueous layer) and insoluble fractions by 15,000 rpm centrifugation at 4°C for 10 minutes. The pellet was subsequently washed three times with 50% methanol and once with 100% methanol to remove polar contaminants. Polar fractions were dried at 10-3 mBar using a SpeedVac (Thermo) and stored at -80º C until derivatization steps were performed. Hydrolysis of the protein/glycogen fraction was performed by first resuspending the dried pellet in ddH_2O, followed by the addition of equal part 6M hydrochloric acid (HCl). Samples were vortexed thoroughly and incubated at 95°C for 2 hours. Hydrolysis was quenched with 100% methanol with 40 μM L-norvaline, samples incubated on ice for 30 minutes, and the supernatant collected after centrifugation at 15,000 rpm at 4°C for 10 minutes. The collected supernatant was subsequently dried by vacuum centrifuge at 10-3 mBar.

Dried polar and glycogen samples were derivatized by the addition of 20 mg/ml methoxyamine hydrochloride in pyridine and incubated for 1.5 hours at 30°C. N-methyl-trimethylsilyl-trifluoroacetamide (MSTFA) was then sequentially added to samples, followed by an incubation time of 30 minutes at 37°C with thorough mixing between addition of solvents. The mixture was then transferred to a v-shaped amber glass chromatography vial and analyzed by gas-chromatography mass spectrometry (GCMS). An Agilent 7800B gas-chromatography coupled to a 5977B mass spectrometry detector was used for this study. GCMS protocols were similar to those described previously[25,26], except a modified temperature gradient was used for GC: the initial temperature was 130°C, held for 4 minutes, rising at 6°C/minutes to 243°C, then rising at 60°C/minutes to 280°C, and held for 2 minutes. The electron ionization (EI) energy was set to 70 eV. Scan (m/z:50-800) and full scan mode was used for metabolomics analysis. Mass spectra were translated to relative metabolite abundance using the Automated Mass Spectral Deconvolution and Identification System (AMDIS) software matched to the FiehnLib metabolomics library (available through Agilent) for retention time and fragmentation pattern. Quantitation was performed using the software Mnova (Mestrelab) with a primary ion and at least two or more matching qualifying ions. Relative abundance was corrected for recovery using the L-norvaline standard and adjusted to protein input.

Data collection and statistical analysis

For the biochemical analyses, image quantification and behavioral assessment of seizure susceptibility after kainate administration, computed results were processed for statistical analysis with PRISM 8.0 (GraphPAD Software, San Diego, USA). Data are represented as the mean±SEM. Normality of the distributions was checked via the Shapiro–Wilk test. All the tests performed were two-sided. Statistical significance of differences between groups was inferred by Student's t-Test or Two-way ANOVA, followed by the Bonferroni *post-hoc* comparison for all pairwise multiple comparison procedures. Statistical significance was set at $P < 0.05$.

RESULTS

Accumulation of glycogen is prevented in young malin^{KO}+MGS$^{Gfap\text{-}KO}$ mice

To generate a mouse model of LD that is unable to accumulate glycogen specifically in astrocytes, we bred malin^{KO} mice[13,18] with an astrocyte-specific knockout of MGS[5] to obtain malin^{KO}+MGS$^{Gfap\text{-}KO}$ animals. We examined the accumulation of glycogen in the brains of young (3-month-old) malin^{KO}+MGS$^{Gfap\text{-}KO}$ animals, an age at which malin^{KO} mice already show a great number of LBs in this organ. To this end, PAS staining and MGS immunostaining were performed in coronal brain sections, and total brain glycogen content was biochemically quantified. A considerable number of glycogen aggregates were observed in malin^{KO} brains after PAS staining and MGS immunostaining, as previously reported[13]. In contrast, malin^{KO}+MGS$^{Gfap\text{-}KO}$ animals showed a dramatic reduction in the number of aggregates (Figure 1A). The biochemical determination of glycogen content also revealed an increase in the brains of malin^{KO} mice ($P < 0{,}0001$) while glycogen levels in malin^{KO}+MGS$^{Gfap\text{-}KO}$ brains were lower than those of wild-type controls ($P < 0{,}0001$) (Figure 1B).

Malin^{KO}+MGS$^{Gfap\text{-}KO}$ mice accumulate nLBs but not CAL

We previously reported that most aggregates that accumulate in malin^{KO} hippocampi correspond to astrocytic CAL, although some nLBs were detected in the CA2-CA3 region[19]. As expected, the hippocampi of malin^{KO}+MGS$^{Gfap\text{-}KO}$ brains contained

nLBs but were devoid of CAL (Figure 2, top panels). Likewise, nLBs, but not CAL, were present in the cortices of malin^{KO}+MGS$^{Gfap\text{-}KO}$ animals (Figure 2, central panels). The cerebella of malin^{KO}+MGS$^{Gfap\text{-}KO}$ mice were almost completely free of the glycogen aggregates typical of malin^{KO} cerebella, thereby indicating that these aggregates were mainly astrocytic CALs (Figure 2, lower panels). These results confirm that most brain LBs are in fact astrocytic and that they correspond to the CAL morphology[19].

Western blot analyses of brain extracts

We next analyzed the levels of MGS and laforin in brain extracts of the different groups by Western blot. MGS and laforin were increased in the brains of young malin^{KO} animals (P = 0,0056 and P = 0,0407, respectively), reproducing the results previously reported for older animals[13,18]. In contrast, in the brains of young malin^{KO}+MGS$^{Gfap\text{-}KO}$ mice, MGS levels were decreased and laforin showed normal levels (P = 0,0002 and P = 0,7056, respectively). These findings thus indicate that the accumulation of these proteins in malin^{KO} brains takes place mainly in astrocytes (Figure 3). In older malin^{KO} brains, the autophagy adaptor p62 is increased, which has been described as an indicator of autophagy impairment in these animals[29]. We found that young malin^{KO} animals also presented an increase in p62 levels in the brain (P = 0,0002). Importantly, p62 levels were normalized in malin^{KO}+MGS$^{Gfap\text{-}KO}$ animals (P < 0,0001 with respect malin^{KO}), thereby indicating again that this increase was due mainly to the astrocytic population (Figure 3).

Assessment of pathology in aged malin^{KO}+MGS$^{Gfap\text{-}KO}$

The results described thus far established that most LBs in malin^{KO} brains accumulate in astrocytes. We next analyzed whether these astrocytic LBs contribute to the pathology of LD. Three-month-old malin^{KO} animals do not show signs of brain damage, which appear at older ages[18,30]. We therefore used 11-month-old animals from the different groups to dissect the specific contribution of glycogen accumulation in astrocytes to the pathology of the disease. The analysis of this process in the brains of these aged groups reproduced the results obtained with younger animals (Supplementary Figure 1). Old malin^{KO}+MGS$^{Gfap\text{-}KO}$ mice presented

nLBs, but not CALs (Supplementary Figure 1A), and low levels of brain glycogen, while malin^{KO} brains showed a clear increase in glycogen with respect to controls (Supplementary Figure 1B). Western blot analyses also revealed increased levels of MGS, laforin and p62 in malin^{KO} brains. In contrast, these parameters were reduced in the brains of malin^{KO}+MGS$^{Gfap\text{-}KO}$ animals (Supplementary Figure 1C).

Histological markers, namely Gfap for astrogliosis and Iba-1 for microgliosis, have been widely used to assess brain damage in LD mouse models[13,14,30-32]. The analysis of these markers showed increased staining in aged malin^{KO} brains (Gfap (P < 0,0001), Iba1 (P = 0,0024)), as we previously described[9]. The increase was particularly prominent in the hippocampus, a region that accumulates numerous CAL[4]. Strikingly, the levels of these markers were normalized in the brains of malin^{KO}+MGS$^{Gfap\text{-}KO}$ mice (Gfap (P = 0,2993), Iba1 (P = 0,8521)) (Figure 4A,B). In line with these histological markers, the upregulation of genes encoding mediators of the inflammatory response has also been reported in mouse models of LD[18]. The analysis some of these genes, namely C3, Ccl2, Lcn2 and Cxcl10, by qPCR confirmed the upregulation of their expression in malin^{KO} brains (P = 0,0006, P = 0,0051, P = 0,0083 and P = 0,0015, respectively). Consistent with the histological results, the expression of these genes was similar to normal levels in malin^{KO}+MGS$^{Gfap\text{-}KO}$ brains (P = 0,1098, P = 0,0325, P = 0,2041 and P = 0,3590, respectively) (Figure 4C). Cumulatively, these results indicate that astrogliosis and microgliosis in malin^{KO} brains are mainly a result of the accumulation of glycogen in astrocytes.

Glycogen overaccumulation in astrocytes *per se* induces astrogliosis and neuroinflammation

After the above results, we next examined whether the overaccumulation of glycogen in astrocytes *per se* induces the changes in brain damage markers that we described in malin^{KO} brains. To this end, we took advantage of our animal model, in which a non-inactivatable form of MGS (9A-MGS) can be expressed in a cell-type specific manner[17]. We crossed this mouse model with Gfap-Cre mice to induce the accumulation of glycogen in astrocytes (9A-MGS^{Gfap}). PAS staining, MGS

immunostaining and biochemical determination of glycogen in the brains of 3-month-old 9A-MGS^{Gfap} mice revealed a conspicuous accumulation of glycogen ($P < 0,0001$) (Figure 5A, B). Western blot analyses in total brain homogenates of these mice revealed that MGS overexpression was accompanied by an increase in laforin, thereby mimicking the results obtained in the brains of malin^{KO} mice. Also, the autophagy marker p62 showed increased levels in the brains of 9A-MGS^{Gfap} mice (Figure 5C).

We analyzed the presence of Gfap and Iba-1 in these brains. Interestingly, both markers were dramatically increased in 9A-MGS^{Gfap} animals when compared to control littermates ($P = 0,0016$ and $P = 0,0005$, respectively) (Figure 6A,B). These results indicate that the accumulation of glycogen in astrocytes *per se* induces astrogliosis and microgliosis. The inflammatory phenotype in the 9A-MGS^{Gfap} model was again confirmed by qPCR analysis of genes involved in the inflammatory response (C3 ($P < 0,0001$), Ccl2 ($P = 0,0027$), Lcn2 ($P < 0,0001$) and Cxcl10 ($P < 0,0001$)) (Figure 6C). Taken together, the results obtained with the 9A-MGS^{Gfap} mice confirm that the overaccumulation of glycogen in astrocytes *per se* induces brain damage.

Analysis of susceptibility to kainate-induced epilepsy in malin^{KO}+MGS$^{Gfap\text{-}KO}$

The accumulation of LBs in malin^{KO} brains also leads to increased susceptibility to kainate-induced epilepsy[13,18], which is in accordance with early LD symptoms. To analyze the contribution of astrocytic LBs to this epileptic phenotype, we measured the susceptibility of malin^{KO} and malin^{KO}+MGS$^{Gfap\text{-}KO}$ animals to kainate-induced seizure. Mice received three consecutive kainate injections (8 mg/kg, i.p. every 30 min) and were video-recorded for 180 minutes after the first injection to monitor their behaviour (i.e. epileptic events). Mice from the three groups reached similar severity stages. However, an increased proportion of malin^{KO} and malin^{KO}+MGS$^{Gfap\text{-}KO}$ animals reached the highest severity stages (V and VI, Figure 7A). Analysis of the time spent in each stage revealed that malin^{KO} mice spent significantly less time in stages I to IV ($P = 0,035$) and more time in stage VI ($P = 0,051$) when compared to control animals, indicating an increased susceptibility to kainate-induced seizures.

Malin^{KO}+MGS$^{Gfap\text{-}KO}$ animals were positioned in between the two groups, not being significantly different from either control or malin^{KO} animals in any stage (Figure 7B). Similarly, when we analysed the number of seizures per animal correlated by time, we found significant differences between control and malin^{KO} animals after the third kainate administration (P = 0,002), with malin^{KO}+MGS$^{Gfap\text{-}KO}$ animals again showing an intermediate response in between the two genotypes (Figure 7C). In summary, malin^{KO} mice were more susceptible to kainate-induced epilepsy with respect to control littermates, as previously reported. This increase was not significantly reduced in malin^{KO}+MGS$^{Gfap\text{-}KO}$ mice. This observation thus indicates that astrocytic LBs are not the main driver of the increase in the susceptibility to kainate-induced epilepsy in malin^{KO} animals.

Metabolomic profiles

Neurophysiological impairments are difficult to detect in LD mouse models[12,33,34], and recent work demonstrated that LD causes changes in the cerebral metabolome[26]. Therefore, we used the LD brain metabolic signature to assess disease status. To this end, we used gas chromatography-mass spectrometry (GC-MS) to define the cerebral metabolome of malin^{KO}, malin^{KO}+MGS$^{Gfap\text{-}KO}$ and control animals. We performed targeted metabolomics analysis of central carbon metabolites involved in glycolysis, the pentose phosphate pathway (PPP), the TCA cycle, and amino acid metabolism. Using this information-rich metabolomics dataset, we performed supervised clustering analysis to assess the overall metabolic profiles. In line with our hypothesis, distinct clustering was observed between malin^{KO} animals and control animals (Fig. 8A). Importantly, the malin^{KO}+MGS$^{Gfap\text{-}KO}$ mice clustered and partially overlapped with the control animals, demonstrating a partial normalization of brain metabolism. Corroborating these findings, similar trends were observed using Ward hieratical cluster analysis, where malin^{KO}+MGS$^{Gfap\text{-}KO}$ more closely clustered with control rather than malin^{KO} mice (Fig. 8B). Additionally, metabolites used to generate these analyses were related to glycogen metabolism, glycolysis, TCA cycle, and amino acids (Fig. 8B). Taken together, these data strongly suggest that astrocytic LBs are the main contributors to the metabolic alterations present in malin^{KO} mice.

DISCUSSION

LD is a devastating condition for which there is no current treatment. Demonstration that the accumulation of glycogen in the nervous system underlies the pathophysiology of the disease identified glycogen synthase as a druggable target and opened up the possibility of designing potential treatments[26,35]. Traditionally, it was considered that under normal conditions glycogen is present exclusively in astrocytes[36], while in LD, LBs accumulate exclusively in neurons[16]. These two concepts represented a paradox that was difficult to understand. However, we first demonstrated that neurons have an active glycogen metabolism[3,4], which explains why they can accumulate aberrant glycogen in conditions like LD. Also, we[13,19] and others[20] showed that LBs are not exclusive to neurons and that astrocytes also accumulate these aggregates in LD. Here we reveal that the accumulation of glycogen aggregates in astrocytes contributes to the pathophysiology of LD.

The analysis of the LBs present in malin^{KO}+MGS$^{Gfap\text{-}KO}$ brains demonstrates that the vast majority of aggregates accumulate in astrocytes, thereby confirming our previous indirect results obtained by colocalization with neuronal and astrocytic markers[19]. Furthermore, biochemical quantification showing low levels of glycogen in the brains of malin^{KO}+MGS$^{Gfap\text{-}KO}$ mice also indicates that neuronal LBs represent a very small fraction of the glycogen accumulated in malin^{KO} brains. LBs have traditionally been classified into type I, type II and type III subtypes. The first type accounts for the largest proportion of total LBs, they affect the neuropil and they are granular, polymorphic, "dust-like" particles. In contrast, type II LBs and the more rare type III are bigger and spherical and they are always located in the neuronal perikaryon[16,37]. On the basis of these characteristics, type I LBs correspond to CAL, and type II and III to nLBs[19]. It has been hypothesized that type II LBs are formed only when the production of type I LBs is insufficient to contain the polyglucosans generated[16]. In the light of our results, this hypothesis can be discarded, since type I and type II LBs are in fact generated in different cell types, i.e. type I LBs in astrocytes and type II and III in neurons. Along the same line, our results demonstrate that astrocytic LBs

are formed in the astrocytes themselves and do not derive from neurons. Likewise, they show that neurons generate LBs and do not import them from astrocytes.

Neuropathology has classically been dominated by neuron-centric views, in which pathology is focused on the survival or death of neurons. However, astrocytes are emerging as a central element of neuropathology. Astrocytes play essential roles in brain function[38,39], and astrocytic dysfunction has been shown to contribute to the pathology of disorders like Alzheimer's disease[40], Huntington's disease[41], Parkinson's disease[42,43] and Amyotrophic Lateral Sclerosis[44]. However, whether astrocytic dysfunction reflects cell-autonomous mechanisms in these diseases is not clear yet. Neuroinflammation is one of the most important traits in the pathophysiology of LD[30]. Here we show that neuroinflammation is corrected in malin^{KO}+MGS$^{Gfap\text{-}KO}$ mice, as shown by Gfap and Iba-1 immunostaining, as well as by the expression of genes encoding mediators of the inflammatory response. In line with these observations, 9A-MGS^{Gfap} animals showed clear signs of neuroinflammation. Although in this model the accumulation of glycogen in astrocytes is very high, and thus it does not faithfully mimic LD, these results indicate that the overaccumulation of glycogen in astrocytes *per se* induces this pathophysiological trait. Furthermore, autophagy markers were also normalized in malin^{KO}+MGS$^{Gfap\text{-}KO}$ brains and altered in 9A-MGS^{Gfap} brains. These findings indicate that dysfunctions in autophagy, which had been proposed as the underlying cause of LD[11,45], also occur mainly in astrocytes. Similarly, our metabolomics analyses indicated that the metabolic alterations characteristic of malin^{KO} brains are partially corrected in malin^{KO}+MGS$^{Gfap\text{-}KO}$ brains. These results demonstrate not only that the impairment of astrocytic function plays a role in the pathophysiology of LD but that it is a primary role, resulting from the accumulation of LBs in the astrocytes themselves, and not a secondary role derived of the accumulation of neuronal LBs. Our findings unveil astrocytes as a key target in the treatment of LD and make LD one of the few examples of neurodegenerative diseases in which a cell-autonomous dysfunction of astrocytes has been demonstrated.

Targeted metabolomics analyses and supervised clustering analysis revealed rescue of a wide range of interconnecting metabolic pathways. These include central carbon

metabolic pathways (hexose and lactate), amino acid metabolism (glycine and cysteine), and lipid metabolism (lactamide). Thus, these data suggest a change in malin^{KO}+MGS$^{Gfap\text{-}KO}$ brain metabolism towards control metabolism. Brain metabolism is the biochemistry that underlines brain physiology, and shifts within these pathways towards control levels suggest partial rescue of the diseased phenotype. However, the total pooled metabolites analyzed here only represent a change in metabolism. Isotopic tracing is required to obtain detailed flux data such as substrate utilization and direction of change for each individual pathway.

The many roles of astrocytes in the regulation of neuronal excitability make them key players in the pathogenesis of epilepsy[46,47]. Furthermore, neuroinflammation, which is rescued in malin^{KO}+MGS$^{Gfap\text{-}KO}$ mice, has been shown to play a role in epileptogenesis[48]. For these reasons, we examined whether the accumulation of LBs in astrocytes also underlies the epileptic phenotype of LD. However, susceptibility to kainate-induced epilepsy was not rescued in malin^{KO}+MGS$^{Gfap\text{-}KO}$ mice. Indeed, these mice showed only a minor improvement in the number and severity of seizures, which could be due to the absence of neuroinflammation. These results therefore strongly suggest that astrocytic LBs are not the main contributors to the increased susceptibility to kainate-induced epilepsy, and thus this pathological trait would be more attributable to neurons. In this regard, deletion of PPP1R3D in mouse model of LD leads to reduced nLBs and a trend toward decreased susceptibility to kainate-induced seizures[49].

The results presented here are consistent with those reported for adult polyglucosan body disease (APBD), in which accumulation of abnormal glycogen in astrocytes is sufficient to cause the disease[50]. Interestingly, APBD patients share symptoms with LD, like dementia, but they do not present an epileptic phenotype. These data again suggest that the LD epilepsy derives from the accumulation of aberrant glycogen in neurons.

The accumulation of aberrant glycogen in astrocytes is not exclusive to LD and APBD. Aging and some neurodegenerative conditions (including Alzheimer's,

Huntington's, Parkinson's and Pick's diseases) also lead to the appearance of astrocytic glycogen aggregates known as corpora amylacea[51,52]. Thus, the results presented here will impact beyond LD and open up the question of whether glycogen accumulation in astrocytes contributes to the cognitive decline associated with aging and to the pathology of these other neurodegenerative diseases.

In summary, our results shed new light on the pathophysiological bases of LD, moving it from a neurocentric perspective to one in which astrocytes are also key players. Based on the results presented here, we propose that the accumulation of CAL in astrocytes underlies autophagy impairment, metabolic alterations and neuroinflammation, while epilepsy is mainly the result of nLB-induced neuronal dysfunction. By expanding a growing body of evidence supporting the involvement of glial cells in neurodegenerative diseases, our results have important implications for the design of treatments for LD and other disorders.

DATA AVAILABILITY STATEMENT

Raw data and images are available upon request from the corresponding author.

ACKNOWLEDGEMENTS

The authors thank Anna Adrover and Emma Veza for technical assistance. Thanks also go to Tanya Yates for correcting the English manuscript.

FUNDING INFORMATION

IRB Barcelona and IBEC are the recipient of a Severo Ochoa Award of Excellence from MINECO (Government of Spain). This study was supported by grants from MINECO (BFU2017-84345-P to JD and JJG and RTI2018-099773-B-I00 to JADR and AH), the CIBER de Diabetes y Enfermedades Metabólicas Asociadas (ISCIII, Ministerio de Ciencia e Innovación), a grant from the National Institutes of Health (NIH-NINDS) (P01 NS097197) to JJG and MSG, NIH grant R35 NS116824 to MSG, and NIH grant R01 AG066653 to RS. The project leading to these results also

received funding from “la Caixa” Foundation (ID 100010434) under the agreement LCF/PR/HR19/52160007 with JADR.

COMPETING INTERESTS

The authors report no competing interests.

REFERENCES

1. Duran J, Saez I, Gruart A, Guinovart JJ, Delgado-Garcia JM. Impairment in long-term memory formation and learning-dependent synaptic plasticity in mice lacking glycogen synthase in the brain. *J Cereb Blood Flow Metab.* Apr 2013;33(4):550-556.

2. Lopez-Ramos JC, Duran J, Gruart A, Guinovart JJ, Delgado-Garcia JM. Role of brain glycogen in the response to hypoxia and in susceptibility to epilepsy. *Frontiers in cellular neuroscience.* 2015;9:431.

3. Saez I, Duran J, Sinadinos C, et al. Neurons have an active glycogen metabolism that contributes to tolerance to hypoxia. *J Cereb Blood Flow Metab.* Jun 2014;34(6):945-955.

4. Duran J, Gruart A, Varea O, Lopez-Soldado I, Delgado-Garcia JM, Guinovart JJ. Lack of Neuronal Glycogen Impairs Memory Formation and Learning-Dependent Synaptic Plasticity in Mice. *Frontiers in cellular neuroscience.* 2019;13:374.

5. Duran J, Brewer MK, Hervera A, et al. Lack of Astrocytic Glycogen Alters Synaptic Plasticity but Not Seizure Susceptibility. *Mol Neurobiol.* Nov 2020;57(11):4657-4666.

6. Duran J, Guinovart JJ. Brain glycogen in health and disease. *Molecular aspects of medicine.* Dec 2015;46:70-77.

7. Duran J, Gruart A, Lopez-Ramos JC, Delgado-Garcia JM, Guinovart JJ. Glycogen in Astrocytes and Neurons: Physiological and Pathological Aspects. *Advances in neurobiology.* 2019;23:311-329.

8. Turnbull J, Tiberia E, Striano P, et al. Lafora disease. *Epileptic Disord.* Sep 1 2016;18(S2):38-62.

9. Gentry MS, Guinovart JJ, Minassian BA, Roach PJ, Serratosa JM. Lafora disease offers a unique window into neuronal glycogen metabolism. *J Biol Chem.* May 11 2018;293(19):7117-7125.

10. Gentry MS, Worby CA, Dixon JE. Insights into Lafora disease: malin is an E3 ubiquitin ligase that ubiquitinates and promotes the degradation of laforin. *Proc Natl Acad Sci U S A.* Jun 14 2005;102(24):8501-8506.

11. Singh S, Ganesh S. Lafora progressive myoclonus epilepsy: a meta-analysis of reported mutations in the first decade following the discovery of the EPM2A and NHLRC1 genes. *Hum Mutat.* May 2009;30(5):715-723.

12. Garcia-Cabrero AM, Marinas A, Guerrero R, de Cordoba SR, Serratosa JM, Sanchez MP. Laforin and malin deletions in mice produce similar neurologic impairments. *J Neuropathol Exp Neurol.* May 2012;71(5):413-421.

13. Duran J, Gruart A, Garcia-Rocha M, Delgado-Garcia JM, Guinovart JJ. Glycogen accumulation underlies neurodegeneration and autophagy impairment in Lafora disease. *Hum Mol Genet.* Jun 15 2014;23(12):3147-3156.

14. Turnbull J, DePaoli-Roach AA, Zhao X, et al. PTG depletion removes Lafora bodies and rescues the fatal epilepsy of Lafora disease. *PLoS Genet.* Apr 2011;7(4):e1002037.

15. Pederson BA, Turnbull J, Epp JR, et al. Inhibiting glycogen synthesis prevents lafora disease in a mouse model. *Ann Neurol.* Mar 21 2013.

16. Machado-Salas J, Avila-Costa MR, Guevara P, et al. Ontogeny of Lafora bodies and neurocytoskeleton changes in Laforin-deficient mice. *Exp Neurol.* Jul 2012;236(1):131-140.

17. Duran J, Tevy MF, Garcia-Rocha M, Calbo J, Milan M, Guinovart JJ. Deleterious effects of neuronal accumulation of glycogen in flies and mice. *EMBO Mol Med.* Aug 2012;4(8):719-729.

18. Valles-Ortega J, Duran J, Garcia-Rocha M, et al. Neurodegeneration and functional impairments associated with glycogen synthase accumulation in a mouse model of Lafora disease. *EMBO Mol Med.* Nov 2011;3(11):667-681.

19. Auge E, Pelegri C, Manich G, et al. Astrocytes and neurons produce distinct types of polyglucosan bodies in Lafora disease. *Glia.* Oct 2018;66(10):2094-2107.

20. Rubio-Villena C, Viana R, Bonet J, et al. Astrocytes: new players in progressive myoclonus epilepsy of Lafora type. *Hum Mol Genet.* Apr 1 2018;27(7):1290-1300.

21. Auge E, Duran J, Guinovart JJ, Pelegri C, Vilaplana J. Exploring the elusive composition of corpora amylacea of human brain. *Scientific reports.* Sep 10 2018;8(1):13525.

22. Bankhead P, Loughrey MB, Fernandez JA, et al. QuPath: Open source software for digital pathology image analysis. *Scientific reports.* Dec 4 2017;7(1):16878.

23. Rangel A, Burgaya F, Gavin R, Soriano E, Aguzzi A, Del Rio JA. Enhanced susceptibility of Prnp-deficient mice to kainate-induced seizures, neuronal apoptosis, and death: Role of AMPA/kainate receptors. *J Neurosci Res.* Sep 2007;85(12):2741-2755.

24. Rangel A, Madronal N, Gruart A, et al. Regulation of GABA(A) and glutamate receptor expression, synaptic facilitation and long-term potentiation in the hippocampus of prion mutant mice. *PLoS One.* Oct 26 2009;4(10):e7592.

25. Carulla P, Bribian A, Rangel A, et al. Neuroprotective role of PrPC against kainate-induced epileptic seizures and cell death depends on the modulation of JNK3 activation by GluR6/7-PSD-95 binding. *Mol Biol Cell.* Sep 2011;22(17):3041-3054.

26. Brewer MK, Uittenbogaard A, Austin GL, et al. Targeting Pathogenic Lafora Bodies in Lafora Disease Using an Antibody-Enzyme Fusion. *Cell Metab.* Oct 1 2019;30(4):689-705 e686.

27. Sun RC, Dukhande VV, Zhou Z, et al. Nuclear Glycogenolysis Modulates Histone Acetylation in Human Non-Small Cell Lung Cancers. *Cell Metab.* Nov 5 2019;30(5):903-916 e907.

28. Andres DA, Young LEA, Veeranki S, et al. Improved workflow for mass spectrometry-based metabolomics analysis of the heart. *J Biol Chem.* Feb 28 2020;295(9):2676-2686.

29. Criado O, Aguado C, Gayarre J, et al. Lafora bodies and neurological defects in malin-deficient mice correlate with impaired autophagy. *Hum Mol Genet.* Apr 1 2012;21(7):1521-1533.

30. Lahuerta M, Gonzalez D, Aguado C, et al. Reactive Glia-Derived Neuroinflammation: a Novel Hallmark in Lafora Progressive Myoclonus Epilepsy That Progresses with Age. *Mol Neurobiol.* Mar 2020;57(3):1607-1621.

31. Lopez-Gonzalez I, Viana R, Sanz P, Ferrer I. Inflammation in Lafora Disease: Evolution with Disease Progression in Laforin and Malin Knock-out Mouse Models. *Mol Neurobiol.* Jul 2017;54(5):3119-3130.

32. Rai A, Mishra R, Ganesh S. Suppression of leptin signaling reduces polyglucosan inclusions and seizure susceptibility in a mouse model for Lafora disease. *Hum Mol Genet.* Dec 15 2017;26(24):4778-4785.

33. Ganesh S, Delgado-Escueta AV, Sakamoto T, et al. Targeted disruption of the Epm2a gene causes formation of Lafora inclusion bodies, neurodegeneration, ataxia, myoclonus epilepsy and impaired behavioral response in mice. *Hum Mol Genet.* May 15 2002;11(11):1251-1262.

34. Sanchez-Elexpuru G, Serratosa JM, Sanchez MP. Sodium selenate treatment improves symptoms and seizure susceptibility in a malin-deficient mouse model of Lafora disease. *Epilepsia.* Mar 2017;58(3):467-475.

35. Gentry MS, Afawi Z, Armstrong DD, et al. The 5th International Lafora Epilepsy Workshop: Basic science elucidating therapeutic options and

preparing for therapies in the clinic. *Epilepsy Behav.* Feb 2020;103(Pt A):106839.

36. Cataldo AM, Broadwell RD. Cytochemical identification of cerebral glycogen and glucose-6-phosphatase activity under normal and experimental conditions. II. Choroid plexus and ependymal epithelia, endothelia and pericytes. *J Neurocytol.* Aug 1986;15(4):511-524.

37. Van Hoof F, Hageman-Bal M. Progressive familial myoclonic epilepsy with Lafora bodies. Electron microscopic and histochemical study of a cerebral biopsy. *Acta Neuropathol.* Feb 3 1967;7(4):315-336.

38. Goubard V, Fino E, Venance L. Contribution of astrocytic glutamate and GABA uptake to corticostriatal information processing. *J Physiol.* May 1 2011;589(Pt 9):2301-2319.

39. Bellot-Saez A, Kekesi O, Morley JW, Buskila Y. Astrocytic modulation of neuronal excitability through K(+) spatial buffering. *Neuroscience and biobehavioral reviews.* Jun 2017;77:87-97.

40. Assefa BT, Gebre AK, Altaye BM. Reactive Astrocytes as Drug Target in Alzheimer's Disease. *BioMed research international.* 2018;2018:4160247.

41. Benraiss A, Wang S, Herrlinger S, et al. Human glia can both induce and rescue aspects of disease phenotype in Huntington disease. *Nature communications.* Jun 7 2016;7:11758.

42. Miyazaki I, Asanuma M. Therapeutic Strategy of Targeting Astrocytes for Neuroprotection in Parkinson's Disease. *Curr Pharm Des.* 2017;23(33):4936-4947.

43. Kuter K, Olech L, Glowacka U, Paleczna M. Astrocyte support is important for the compensatory potential of the nigrostriatal system neurons during early neurodegeneration. *J Neurochem.* Jan 2019;148(1):63-79.

44. Yamanaka K, Komine O. The multi-dimensional roles of astrocytes in ALS. *Neurosci Res.* Jan 2018;126:31-38.

45. Puri R, Suzuki T, Yamakawa K, Ganesh S. Dysfunctions in endosomal-lysosomal and autophagy pathways underlie neuropathology in a mouse model for Lafora disease. *Hum Mol Genet.* Jan 1 2012;21(1):175-184.

46. Coulter DA, Steinhauser C. Role of astrocytes in epilepsy. *Cold Spring Harbor perspectives in medicine.* Mar 2 2015;5(3):a022434.

47. Boison D, Steinhauser C. Epilepsy and astrocyte energy metabolism. *Glia.* Jun 2018;66(6):1235-1243.

48. Rana A, Musto AE. The role of inflammation in the development of epilepsy. *J Neuroinflammation.* May 15 2018;15(1):144.

49. Israelian L, Nitschke S, Wang P, et al. Ppp1r3d deficiency preferentially inhibits neuronal and cardiac Lafora body formation in a mouse model of the fatal epilepsy Lafora disease. *J Neurochem.* Sep 6 2020.

50. Dainese L, Monin ML, Demeret S, et al. Abnormal glycogen in astrocytes is sufficient to cause adult polyglucosan body disease. *Gene.* Feb 25 2013;515(2):376-379.

51. Pirici I, Margaritescu C, Mogoanta L, et al. Corpora amylacea in the brain form highly branched three-dimensional lattices. *Romanian journal of morphology and embryology = Revue roumaine de morphologie et embryologie.* 2014;55(3 Suppl):1071-1077.

52. Rohn TT. Corpora Amylacea in Neurodegenerative Diseases: Cause or Effect? *International journal of neurology and neurotherapy.* 2015;2(3).

FIGURE LEGENDS

Figure 1. Accumulation of glycogen in the brains of 3-month-old mice. LBs are abundant in malin^{KO} hippocampi but greatly diminished in malin^{KO}+MGS$^{Gfap\text{-}KO}$ hippocampi. (A) Low and high power photomicrographs illustrating the distribution of LBs after Periodic acid-Schiff (PAS) staining and MGS immunostaining of the hippocampi of 3-month-old littermates from the different groups. Scale bar = 100 μm. (B) Glycogen content of total brain. (control (n = 7), malin^{KO} (n = 7), malin^{KO}+MGS$^{Gfap\text{-}KO}$ (n = 6)). Data are expressed as mean±S.E.M. ****P<0.0001.

Figure 2. Malin^{KO}+MGS$^{Gfap\text{-}KO}$ brains contain nLBs but not CAL. MGS immunostainings of the CA3-CA2 region of the hippocampus (top panels), the cortex (medium panels) and the cerebellum (lower panels) of 3-month-old mice. Scale bar = 100 μm.

Figure 3. Accumulation of proteins is prevented in malin^{KO}+MGS$^{Gfap\text{-}KO}$ brains. Western blotting for MGS, laforin and p62 of total brain homogenates of 3-month-old mice. (A) Representative blots. (B) Quantification of the bands normalized to Revert. Data are expressed as mean±S.E.M. *P<0.05. **P<0.01. ***P<0.001. ****P<0.0001. $^{n.s.}$non-significant. (n=4 animals per group). Revert was used as loading control.

Figure 4. Analysis of brain damage in malin^{KO}+MGS$^{Gfap\text{-}KO}$ mice. Neuroinflammation markers are increased in the brains of old malin^{KO} mice but normalized in malin^{KO}+MGS$^{Gfap\text{-}KO}$ mice. (A) Gfap and Iba1 immunostainings of hippocampi from the different groups. (B) Quantification of hippocampal area of the immunostainings. Data are expressed as mean±S.E.M. of percentage of positive pixels (control (n = 5), malin^{KO} (n = 7), malin^{KO}+MGS$^{Gfap\text{-}KO}$ (n = 7)). (C) qPCR analysis of genes involved in the inflammatory response. Data are expressed as mean±S.E.M. of 2ˆΔΔCt in relative units for each genotype analysed (control (n = 5), malin^{KO} (n = 5), malin^{KO}+MGS$^{Gfap\text{-}KO}$ (n = 6)). **P<0.01. ***P<0.001. ****P<0.0001. $^{n.s.}$non-significant.

Figure 5. Accumulation of glycogen in 9A-MGS^{Gfap} mice. (A) PAS staining and MGS immunostaining of 9A-MGS^{Gfap} in consecutive serial coronal sections. (B) Glycogen content of total brain (n=6 animals per group). Data are expressed as mean±S.E.M. ****P<0.0001. (C) Western blotting for MGS, laforin and p62 of total brain homogenates. REVERT was used as loading control.

Figure 6. Analysis of brain damage in 9A-MGS^{Gfap} mice. Neuroinflammation markers are increased in the brains of 9A-MGS^{Gfap} mice. (A) Gfap and Iba1 immunostainings of hippocampi. (B) Quantification of the hippocampal area of the

immunostainings. Data are expressed as mean±S.E.M. of percentage of positive pixels (control (n = 5), 9A-MGS^{Gfap} (n = 6)). (C) qPCR analysis of genes involved in the inflammatory response. Data are expressed as mean±S.E.M. of 2ˆΔΔCt in relative units for each genotype analysed (n=6 animals per group). **P<0.01. ***P<0.001. ****P<0.0001.

Figure 7. Study of kainate-induced epilepsy. 11-month-old mice were subjected to three kainate injections (8 mg/kg every 30'), and epileptic responses were analysed for 180 minutes after the first injection. (A) Percentage of mice reaching seizure stages I to VI and KA-induced mortality. (B) Percentage of time spent in each stage during the course of the experiment. Data are expressed as average ±SEM. N= 6 mice/group. Two-way ANOVA P-values display *post-hoc* Bonferroni differences. (C) Number of seizures experienced per animal divided by time segments after the 1st, 2nd and 3rd kainate injections. Data are expressed as average ±SEM. N = 6 animals per group. Two-way ANOVA P-values display *post-hoc* Bonferroni differences.

Figure 8. Metabolic profiles. (A) Sparse Partial Least Squares - Discriminant Analysis (sPLS-DA) multivariate analysis of control (red), malin^{KO} (blue) and malin^{KO}+MGS$^{Gfap\text{-}KO}$ (green) brains. (B) Heatmap clustering showing the 10 most affected metabolites from sPLS-DA multivariate analysis.

Supplementary Figure 1. Accumulation of glycogen in the brains of 11-month-old mice. Aged animals reproduce the results seen in younger animals. (A) MGS immunostaining of hippocampi from the different groups. Scale bar = 100 μm. (B) Glycogen content of total brain extracts (n=6-7 animals per group). Data are expressed as mean±S.E.M. ***P<0.001. ****P<0.0001. (C) Western blotting for MGS, laforin and p62 of total brain homogenates of 11-month-old mice. Revert was used as loading control.

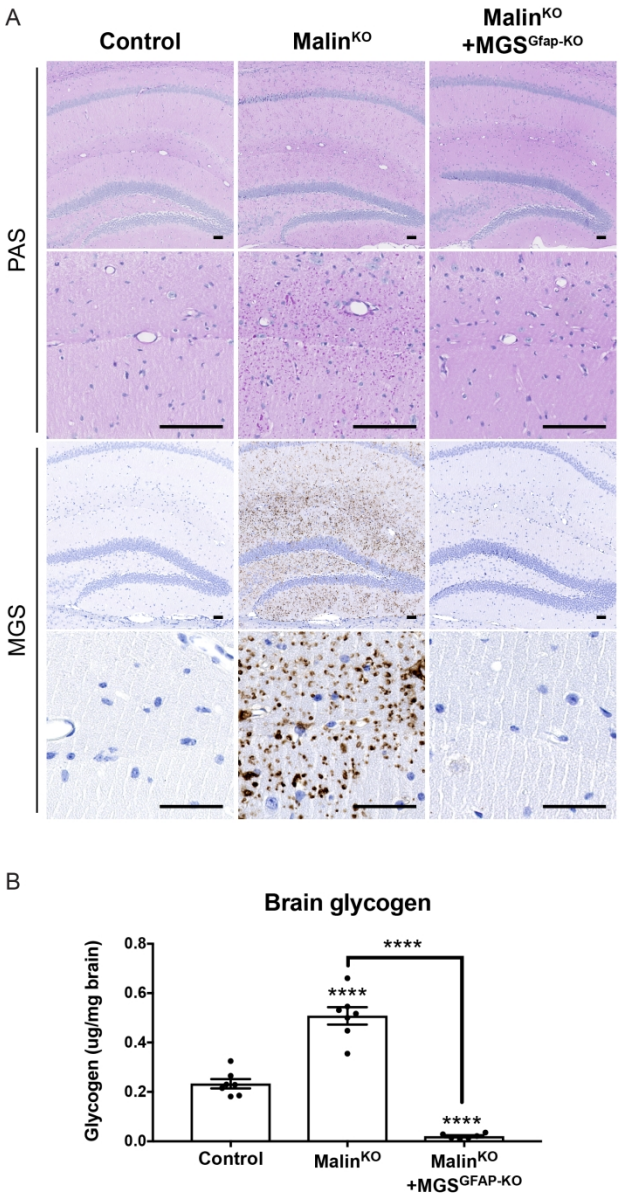

Figure 1. Accumulation of glycogen in the brains of 3-month-old mice. LBs are abundant in malinKO hippocampi but greatly diminished in malinKO+MGSGfap-KO hippocampi. (A) Low and high power photomicrographs illustrating the distribution of LBs after Periodic acid-Schiff (PAS) staining and MGS immunostaining of the hippocampi of 3-month-old littermates from the different groups. Scale bar = 100 µm. (B) Glycogen content of total brain. (control (n = 7), malinKO (n = 7), malinKO+MGSGfap-KO (n = 6)). Data are expressed as mean±S.E.M. ****P<0.0001.

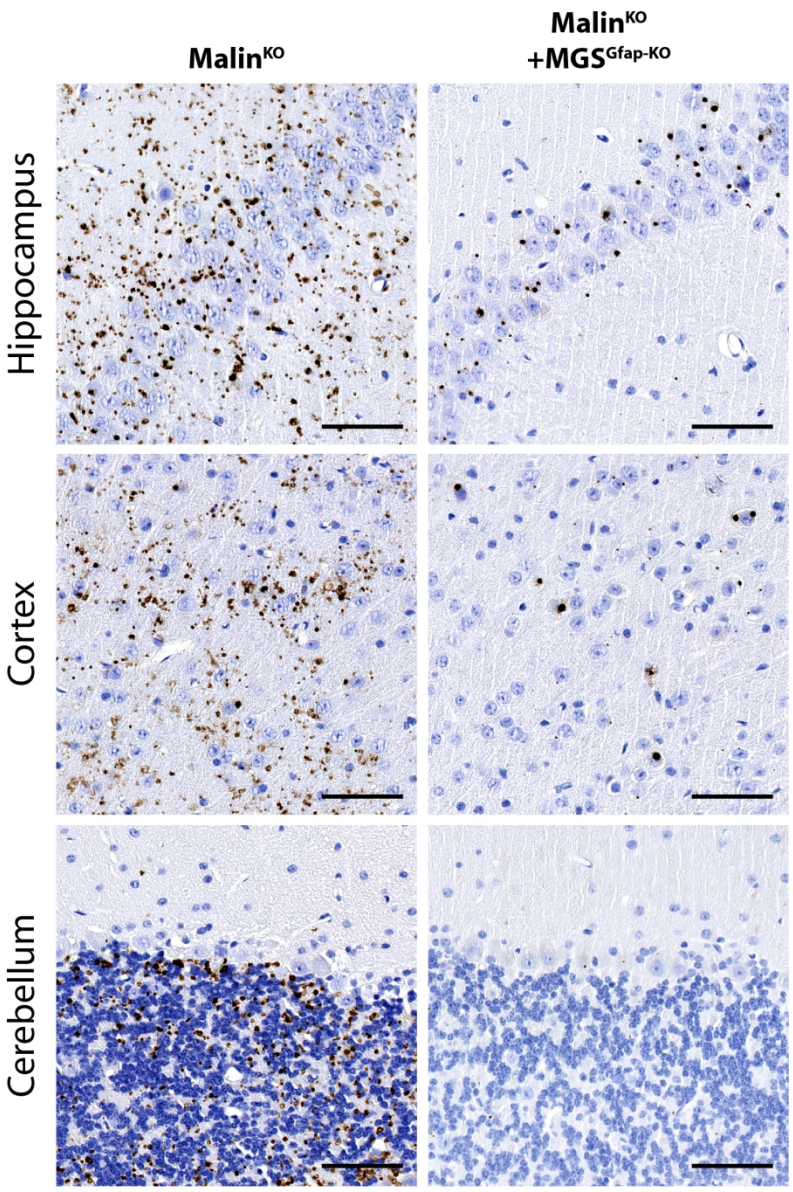

Figure 2. MalinKO+MGSGfap-KO brains contain nLBs but not CAL. MGS immunostainings of the CA3-CA2 region of the hippocampus (top panels), the cortex (medium panels) and the cerebellum (lower panels) of 3-month-old mice. Scale bar = 100 µm.

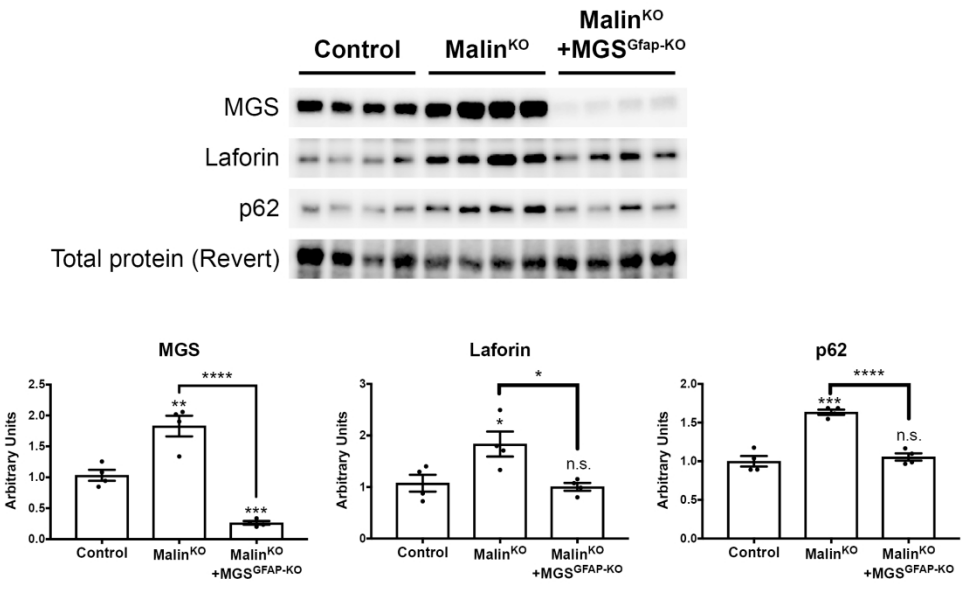

Figure 3. Accumulation of proteins is restored in malinKO+MGSGfap-KO brains. Western blotting for MGS, laforin and p62 of total brain homogenates of 3-month-old mice. (A) Representative blots. (B) Quantification of the bands. Data are expressed as mean±S.E.M. *P<0.05. **P<0.01. ***P<0.001. ****P<0.0001. n.s.non-significant. (n=4 animals per group). Revert was used as loading control.

200x194mm (300 x 300 DPI)

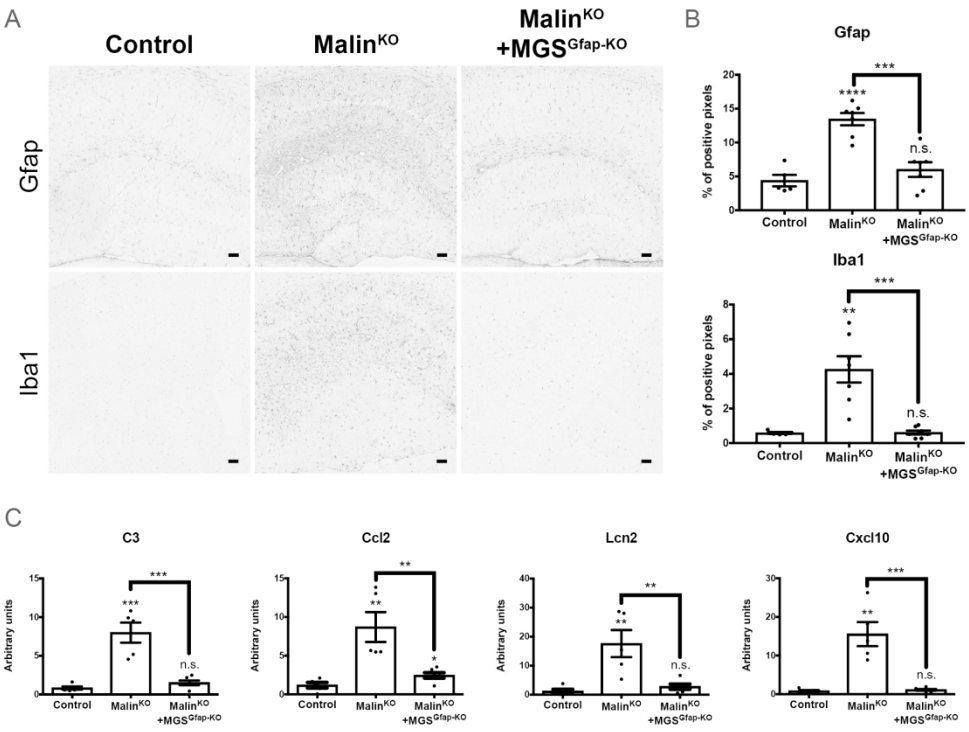

Figure 4. Analysis of brain damage in malinKO+MGSGfap-KO mice. Neuroinflammation markers are increased in the brains of old malinKO mice but normalized in malinKO+MGSGfap-KO mice. (A) Gfap and Iba1 immunostainings of hippocampi from the different groups. (B) Quantification of hippocampal area of the immunostainings. Data are expressed as mean±S.E.M. of percentage of positive pixels (control (n = 5), malinKO (n = 7), malinKO+MGSGfap-KO (n = 7)). (C) qPCR analysis of genes involved in the inflammatory response. Data are expressed as mean±S.E.M. of 2ˆΔΔCt in relative units for each genotype analysed (control (n = 5), malinKO (n = 5), malinKO+MGSGfap-KO (n = 6)). **P<0.01. ***P<0.001. ****P<0.0001. n.s.non-significant.

198x145mm (300 x 300 DPI)

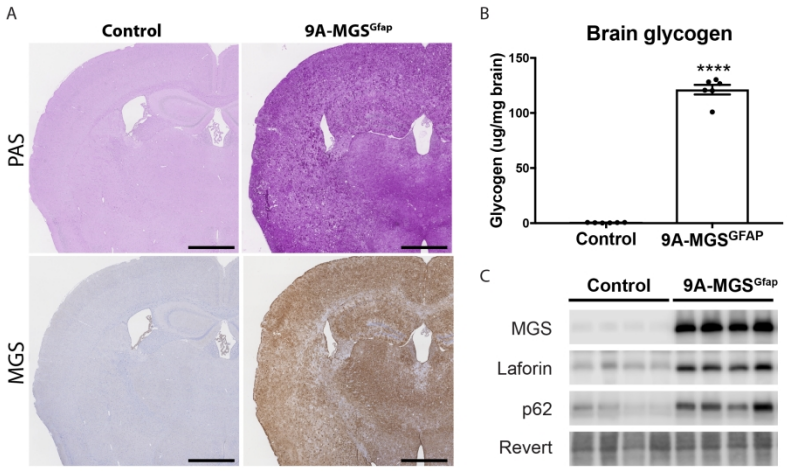

Figure 5. Accumulation of glycogen in 9A-MGSGfap mice. (A) PAS staining and MGS immunostaining of 9A-MGSGfap in consecutive serial coronal sections. (B) Glycogen content of total brain (n=6 animals per group). Data are expressed as mean±S.E.M. ****P<0.0001. (C) Western blotting for MGS, laforin and p62 of total brain homogenates. REVERT was used as loading control.

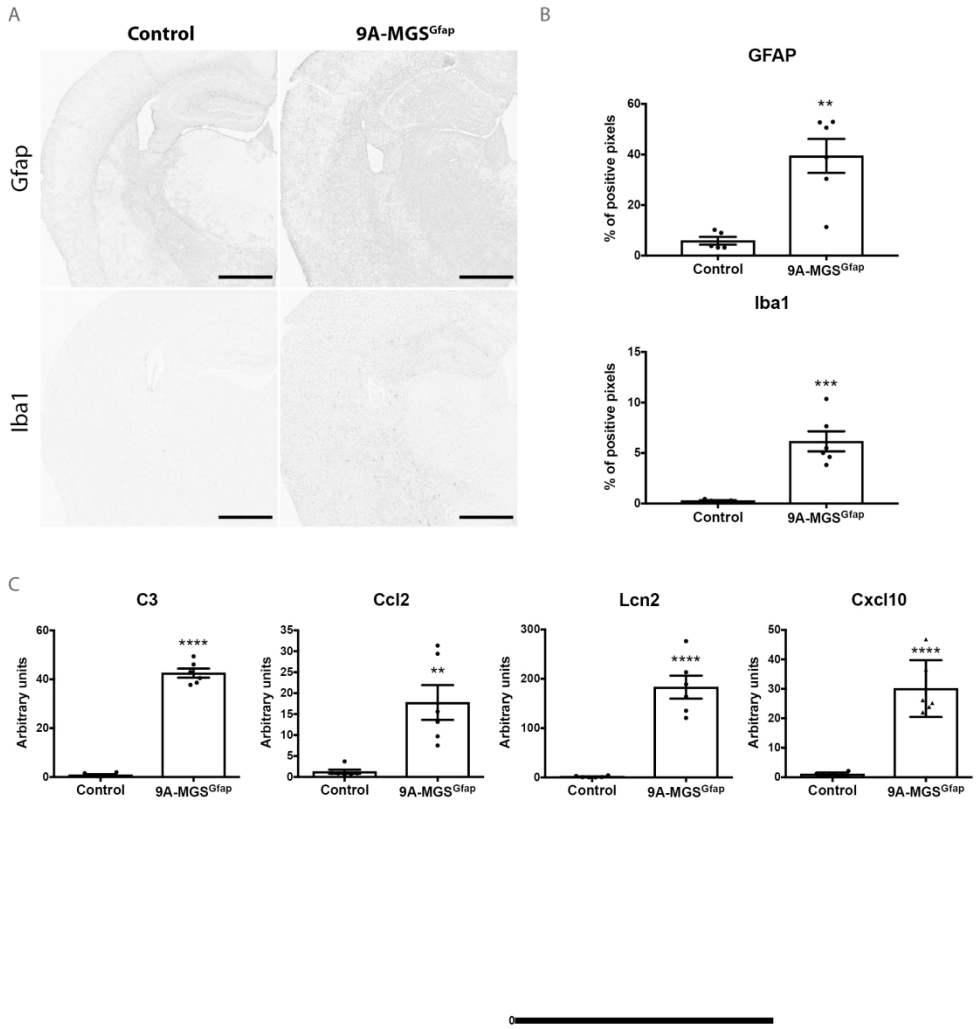

Figure 6. Analysis of brain damage in 9A-MGSGfap mice. Neuroinflammation markers are increased in the brains of 9A-MGSGfap mice. (A) Gfap and Iba1 immunostainings of hippocampi. (B) Quantification of the hippocampal area of the immunostainings. Data are expressed as mean±S.E.M. of percentage of positive pixels (control (n = 5), 9A-MGSGfap (n = 6)). (C) qPCR analysis of genes involved in the inflammatory response. Data are expressed as mean±S.E.M. of 2ˆΔΔCt in relative units for each genotype analysed (n=6 animals per group). **P<0.01. ***P<0.001. ****P<0.0001.

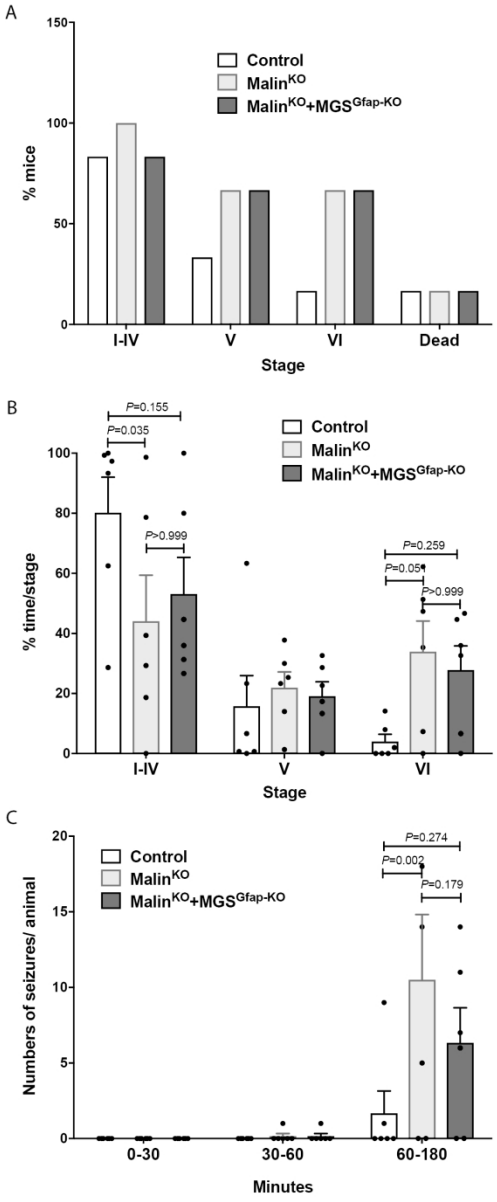

Figure 7. Study of kainate-induced epilepsy. 11-month-old mice were subjected to three kainate injections (8 mg/kg every 30'), and epileptic responses were analysed for 180 minutes after the first injection. (A) Percentage of mice reaching seizure stages I to VI and KA-induced mortality. (B) Percentage of time spent in each stage during the course of the experiment. Data are expressed as average ±SEM. N= 6 mice/group. Two-way ANOVA P-values display post-hoc Bonferroni differences. (C) Number of seizures experienced per animal divided by time segments after the 1st, 2nd and 3rd kainate injections. Data are expressed as average ±SEM. N = 6 animals per group. Two-way ANOVA P-values display post-hoc Bonferroni differences.

111x252mm (300 x 300 DPI)

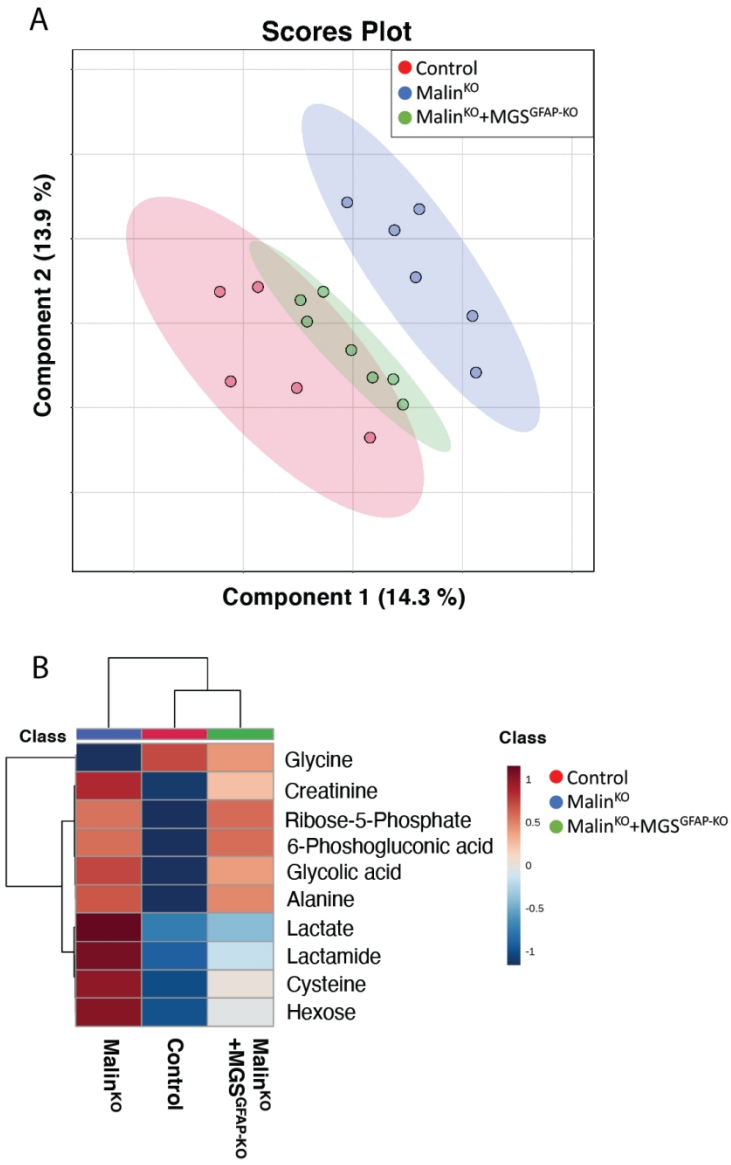

Figure 8. Metabolic profiles. (A) Sparse Partial Least Squares - Discriminant Analysis (sPLS-DA) multivariate analysis of control (red), malinKO (blue) and malinKO+MGSGfap-KO (green) brains. (B) Heatmap clustering showing the 10 most affected metabolites from sPLS-DA multivariate analysis.

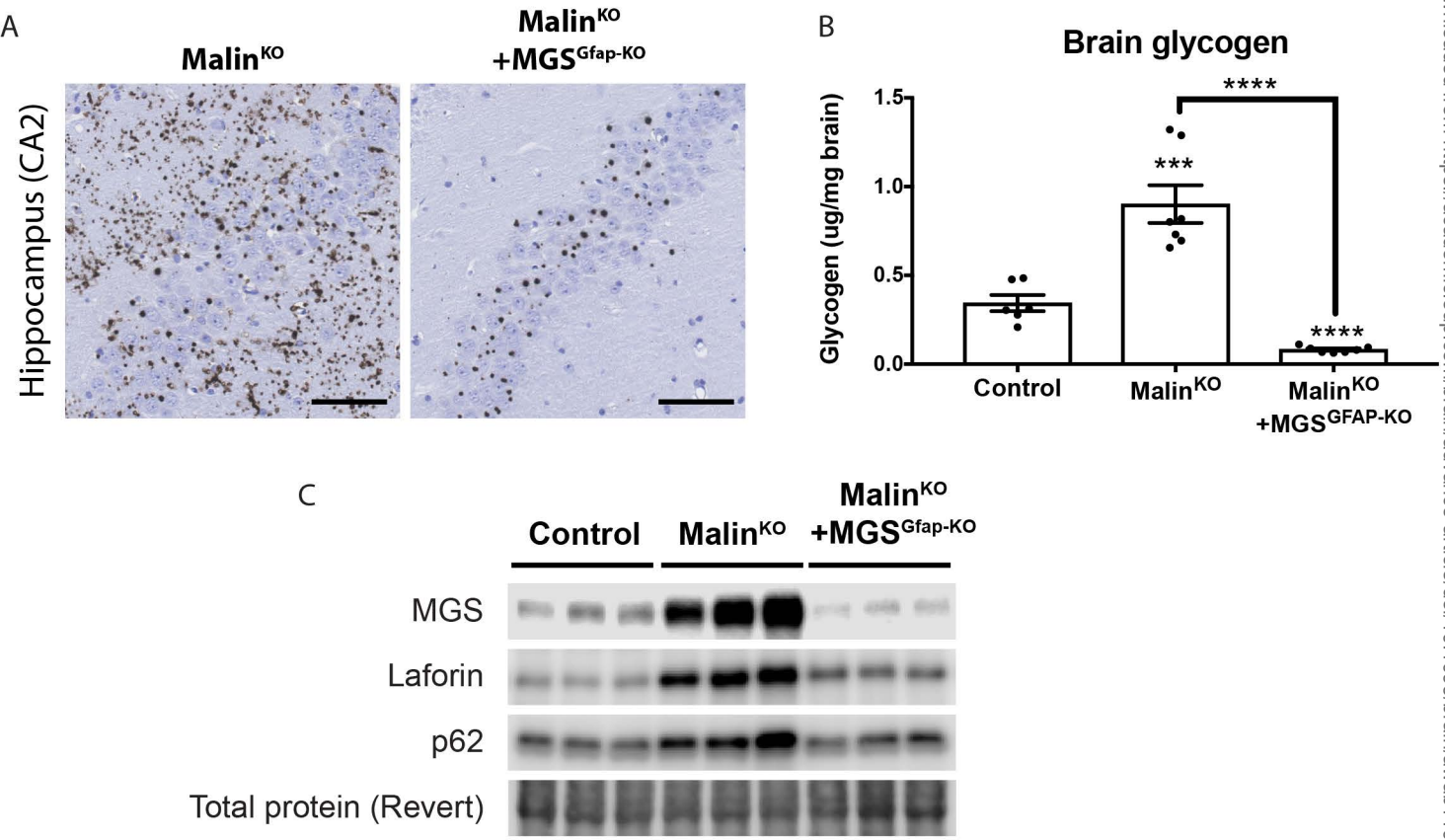

It was believed until recently that Lafora disease pathology derives exclusively from the accumulation of glycogen in the brain in the form of so-called Lafora bodies inside neurons. However, Duran *et al.* now show that it is the accumulation of Lafora bodies inside astrocytes that underlies neurodegeneration in Lafora disease.